Bandgap structure in elastic metamaterials with curvy Bezier beams

View Online   Export Citation   CrossMark

Viacheslav Slesarenko[a] [ID]

AFFILIATIONS

Cluster of Excellence livMatS @FIT—Freiburg Center for Interactive Materials and Bioinspired Technologies, University of Freiburg, Georges-Köhler-Allee 105, D-79110 Freiburg, Germany

Note: This paper is part of the APL Special Collection on Fundamentals and Applications of Metamaterials: Breaking the Limits.
[a]Author to whom correspondence should be addressed: viacheslav.slesarenko@livmats.uni-freiburg.de.
URL: https://slesarenko-lab.com

ABSTRACT

This Letter discusses elastic metamaterials incorporating curved beams in their architecture. Through employing Bezier splines, we reveal a wide versatility of geometrical designs of the unit cells and the consequent programmability of bandgap structures. By analyzing more than ten thousand possible specimens altogether, we highlight the similarity between dynamic properties of metamaterials formed by curves with different geometries defined via three variables only that correspond to the coordinates of control points of the Bezier spline. In particular, we establish the importance of such parameter as effective curve length in defining the probable positions of bandgaps. This study shows, in particular, that the bandgap ratio can reach 71% for metamaterials with proposed curved beams—a noticeable contrast with no bandgaps in their counterpart with straight elements. The employment of the deep learning model enables us to effectively predict passband–stopband structure in such metamaterials with satisfactory accuracy, potentially accelerating the design of metamaterials assembled from versatile unit cells.

According to just one from a wide variety of definitions, metamaterials are artificial materials capable of demonstrating unusual and unconventional behavior, thanks to their involved internal organization.[1] Among different classes of metamaterials, one might distinguish so-called elastic metamaterials—materials with rational internal architecture that gives rise to the various phenomena associated with the propagation of elastic waves.[2] Still, the majority of the studies focus on harnessing intricate structure–properties relationships to facilitate the formation of bandgaps or stopbands—frequency ranges for which waves cannot be sustained by material.[3] The sensitivity of the waves to the structure of the metamaterial is closely associated with its periodic nature. In addition to some aperiodic or quasiperiodic exceptions,[4,5] metamaterials are usually defined by the unit cell—building block that repeats in two or three dimensions.[6] Such periodicity makes possible the realization of Bragg scattering[7] directly associated with the formation of bandgaps for selected frequencies. Additionally, in elastic metamaterials, the phenomenon of local resonance is commonly utilized to adjust the bandgap structure within the lower frequency range.[8,9] In general, the geometry of the unit cell, together with the symmetry group of the repeating pattern, defines the dispersion relations in the metamaterial. Furthermore, the dispersion relations in the elastic metamaterials might be controlled via external deformation, thanks to the changes in geometry[10] and induction of internal elastic stresses.[11] In this regard, one of the common strategies for tuning dispersion properties in metamaterials is based on harnessing the loss of stability.[12]

Loss of stability in periodic structures might lead to the formation of wavy interfaces[13] and, in some cases, to alternating the periodicity of the metamaterial.[14] Such geometric changes significantly alter the dispersion curves and can be employed to control and tune the positions and widths of bandgaps.[15,16] A "curliness" of the resulting geometry obviously makes a significant contribution toward resulting metamaterial behavior. Therefore, the incorporation of the curved elements in the initial design of the elastic metamaterials might be a sound strategy for programming their properties. In this case, even without the external deformation triggering the instability-driven transformations, one might have a wide design space to facilitate the required performance. At the same time, many reported metamaterials are still dominantly based on straight elements[17] or relatively simple geometries,[18] partially due to manufacturing limitations.
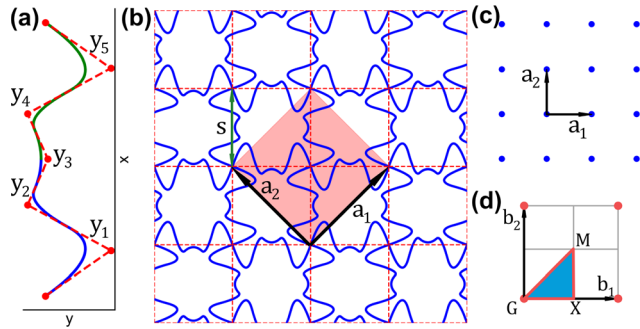
FIG. 1. (a) Bezier curve defined by *y*-coordinates of control points (red). The top half (green) is symmetric with bottom half (blue). (b) The design of elastic metamaterial incorporating Bezier curves. Red square highlights minimal unit cell, while direct lattice basis vectors a_1 and a_2 define the tiling directions. (c) Direct lattice. (d) Reciprocal lattice with highlighted irreducible Brillioun zone (IBZ) and $G - X - M$ perimeter.
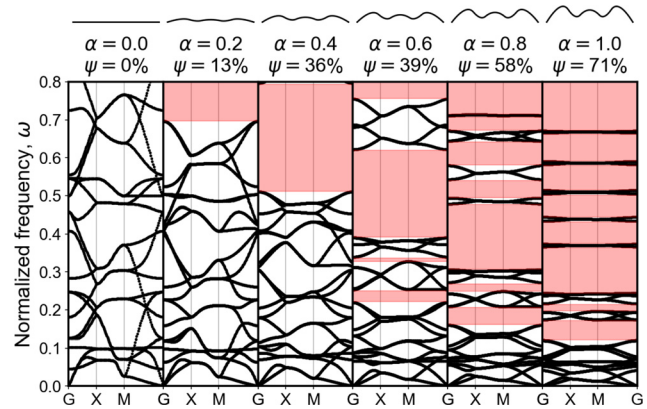

FIG. 2. Dispersion diagrams for the metamaterials assembled from the Bezier curves with different amplitudes. The corresponding curves are shown at the top.

Some exceptions can be found in the case of horseshoe[19] and so-called chiral metamaterials, often incorporating curves in their design.[20] Simultaneously, even for very classical reentrant design, replacement of the straight elements by curvy beams might lead to a very diverse bandgap structure.[21] When necessary for analytical solutions, the replacement non-straight beams are usually defined via relatively simple functions. In contrast, it was recently shown that exploiting more versatile Bezier curves enables better tunability and a wider range of mechanical properties.[22,23] In this Letter, we follow this route and demonstrate the benefits of the Bezier curve for the modification of the classical square lattices in elastic metamaterials.

Bezier splines are continuously differentiable curves that can be obtained recursively.[24] Any Bezier curve is defined by the set of basis functions and by the coordinate of nodes, facilitating a very wide variability of the resulting geometries. In this Letter, we consider Bezier curves of order two with five equidistant nodes [see Fig. 1(a)]. In this case, the five variables $(y_1, y_2, y_3, y_4, y_5)$ reflecting the *y*-coordinate of control points uniquely define the resulting curve and, consequently, the unit cell. Figure 1(b) shows the unit cell of the considered metamaterials that incorporates Bezier curves. If coordinates of control points are selected randomly, the resulting metamaterial belongs to *p4* wallpaper group. To facilitate additional symmetries and generate lattices belonging to the *p4g* group, only Bezier curves with $y_4 = y_2$ and $y_5 = y_1$ were considered, thereby reducing the number of free variables from five to three. To maintain continuity at the nodes, the lattice shown in Fig. 1(b) is assembled from alternating original splines and their mirror counterparts. As one may see, the replacement of the straight beams by curvy ones changes the unit cell, simultaneously increasing its area twofold. To obtain the dispersion diagram for in-plane vibration modes and analyze the stopband–passband structure, we superimposed Bloch–Floquet boundary conditions in COMSOL 5.6 and swept through the perimeter of the Irreducible Brillioun zone (IBZ)[25] [Fig. 1(d)]. The curved beams with end-to-end distance *s* and square cross section of $0.01s^2$ were meshed into at least 50 elements each and modeled under Euler–Bernoulli assumptions. The beams were made of linear elastic materials with Young's modulus $E = 1$ MPa, Poisson's ratio $\nu = 0.4$, and density $\rho = 1000$ kg/m^3. The normalized frequency $\omega = fs/\sqrt{E/\rho}$ was found for wavevector *k* along the perimeter of IBZ, where *f* is the corresponding eigenfrequency. Since ω is

normalized to the lattice period, to simplify further, we assume $s = 1$. To avoid intersections between the neighboring curves, the maximal values of y_i were limited by 0.5. In total, we generated 18000 different geometries of the metamaterial and obtained corresponding dispersion diagrams. To demonstrate the effectiveness of the curved beams in regard to engineering bandgap structure, Fig. 2 compares the dispersion diagrams obtained for the curves defined by coordinates $(y_1, y_2, y_3) = (0.472\alpha, 0.043\alpha, 0.352\alpha)$ for different values of α ranging from 0 to 1. As one may see, in the initial configuration with straight beams, no bandgaps are observed below $\omega = 0.8$. With an increase in the curliness, corresponding dispersion curves shift toward lower frequencies, simultaneously with the opening of the bandgaps at different frequency ranges.

Figure 2 captures only one possible geometry of the Bezier spline. To get a better understanding of the versatility of the geometry–bandgap relationship, we extract two characteristics for each generated metamaterial: length of the base Bezier curve (l_c) and bandgap ratio ψ. Bandgap ratio ψ is defined as $\psi = \sum h_i/\omega_{max} \cdot 100\%$, where h_i is the width of the *i*th bandgap appearing below the maximal frequency of $\omega_{max} = 0.8$. In other words, ψ is the probability of randomly picking the frequency inside the bandgap for the specific metamaterial. We intentionally do not name this value "bandgap width" to avoid confusion with a more common definition of bandgap width.[26] Figure 3(a) shows the dependency of ψ on the length of the used Bezier splines for all considered metamaterials. It is clear that there are multiple curve geometries with the same total length. Simultaneously, for the higher curve lengths l_c, a wider interval of possible ψ (and more versatile bandgap structures) is observed, especially if compared with metamaterial assembled from straight beams. For example, bandgap ratios between 17% and 65% are achievable when the length of the Bezier beam is fixed at $l_c = 2$. The bandgap structures obtained for the metamaterials based on three distinct Bezier curves with $l_c = 2$ are depicted in Fig. 3(b). Significant difference in elastic wave propagation can be observed for metamaterials based on three selected geometries. Note that the restriction on the y_i values forces the upper bound on the maximal length of the Bezier curve equal to 2.84, which corresponds to the vector $\mathbf{y} = (0.5, -0.5, 0.5)$.

Figure 3(c) provides another way of analyzing the bandgap structures for a large set of metamaterials based on Bezier splines. Here, the
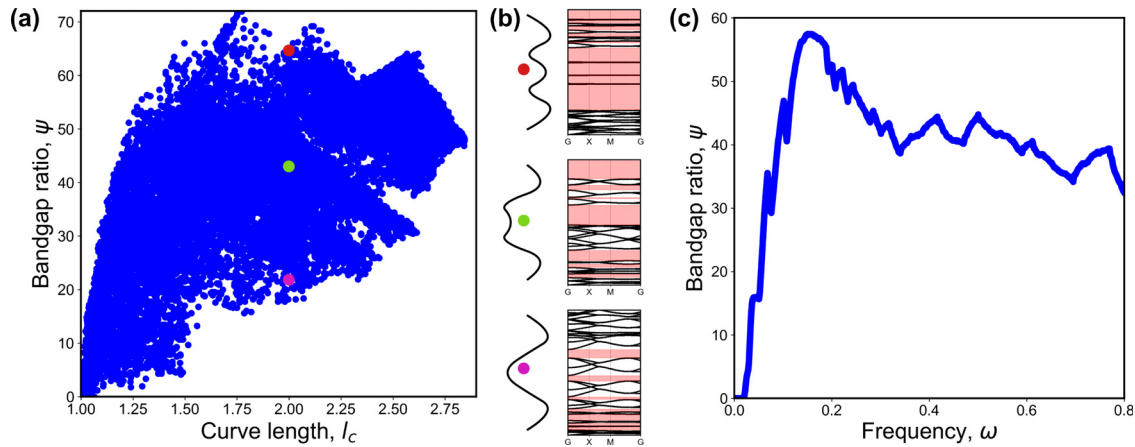
FIG. 3. (a) Dependencies of bandgap ratio ψ on the length of Bezier spline l_c. (b) Dispersion curves of metamaterials formed by three different Bezier curves with the same length of $l_c = 2$. (c) Probability to observe bandgap at the specific frequency for all considered specimens altogether.

probability of observing bandgap ψ is shown as a function of the frequency ω. In other words, the value of the y-axis here corresponds to the probability for randomly selected metamaterial to have bandgap at the frequency ω. One may see that no bandgaps are possible for low enough frequencies ω. This is an expected behavior due to long-wave modes for P- and S-waves that always exist. Simultaneously, different selected frequencies have non-equal probabilities of appearing inside the bandgap zone in considered curvy beams metamaterials. In general, frequencies in the lower diapason of the considered range ($\omega \leq 0.4$) are more likely to be located within the bandgap in comparison with frequencies from the higher half (e.g., $\omega > 0.4$). We associate the observed non-uniform dependency of $\psi(\omega)$ vs ω with the overall geometry of the metamaterial and its periodicity.

Figures 3(a) and 3(c) clearly show the complexity of the relations between the geometry of the base Bezier spline and resulting dispersion diagrams. However, they do not reveal if there is a preference for the exact positions of the stopbands in regard to the curve shape. Considering that here we take into account only curves defined by four intermediate equidistant control points, the earlier introduced curve length l_c remains the dominant geometrical factor. Figure 4 validates this observation by demonstrating contour plot connecting l_c, ω, and $\psi(\omega)$. To generate this plot, the dataset with all generated Bezier splines was split into 93 bins, grouping the curves with similar lengths. Due to the rationally generated dataset, each bin contained exactly 200 splines, resulting in 200 different passband–stopband structures for each bin. The color in Fig. 4 reflects the probability of having a bandgap for the selected frequency ω among the metamaterials generated from the curves of the specific length l_c. First, similar to Fig. 3(c), no bandgaps in any of the considered specimens are observed for very low frequencies represented at the left-most part of the plot. However, the critical minimal value of ω for which the low-frequency bandgap is not observed decreases with an increase in the length of the Bezier spline. Second, it is easy to observe that for each selected curve length l_c, there is a clear differentiation between frequency ranges corresponding to stop- and passbands. In general, an increase in the curve length l_c leads to a continuous decrease in the central frequencies of probable bandgaps, as can be seen in Fig. 4. The relative increase in the bandgap
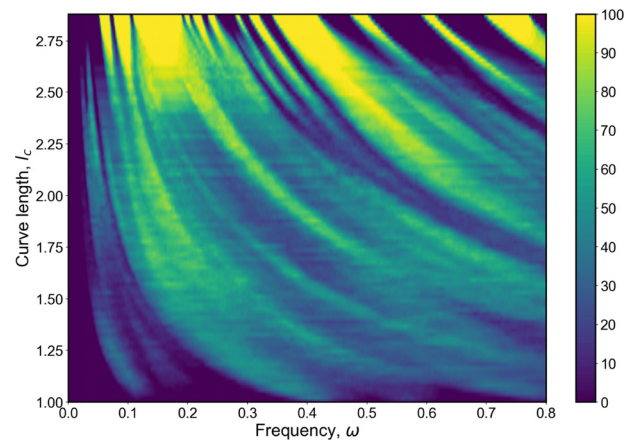

FIG. 4. Contour plot illustrating probability to observe bandgap at the specific frequency ω in metamaterials generated with the help of Bezier curves of length l_c.

probability for the metamaterials employing longer Bezier splines is associated with the lower variability of the curve shapes due to applied limitation on the maximal amplitude (y coordinate of the control points). In general, the shift of the bandgap frequencies toward lower values is associated with an increase in the effective distance between nodes in the resulting metamaterial due to longer connecting Bezier splines.

The intricate relationship between just four input values-coordinates and bandgap structures encourages the employment of machine learning as an efficient replacement for the Bloch–Floquet analysis. The recent advances in deep learning and similar techniques from an area of artificial intelligence enable prediction of the bandgap structures and even inverse design of the metamaterials with desired behavior.[27,28] Every predictive network requires an adequate selection of the input and output variables. While here an obvious input is just a four-element vector $\mathbf{y} = (y_1, y_2, y_3)$ defining the geometry of the Bezier spline, we considered two possible options for output variables. First, in order to fully describe the passband–stopband structure, we
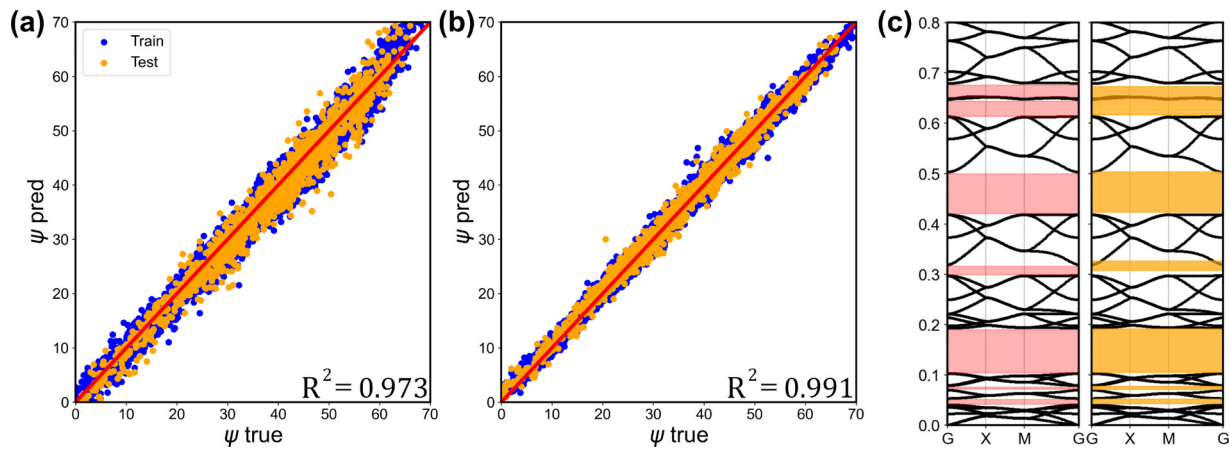
21 August 2023 19:34:03

FIG. 5. (a) Comparison of bandgap ratios ψ obtained via simulations and predicted by a neural network with bandgap vector output. (b) Comparison of bandgap ratios ψ obtained via simulations and predicted by a neural network with single-valued output. (c) Example bandgap structure with highlighted bandgap obtained via simulations (red) and prediction by means of the first neural network (orange).

used the concept of bandgap vector.[27–29] The considered frequency range $0 < \omega \le \omega_{max}$ was split into $n = 500$ narrow frequency bands $\omega_{max} i/n \le \omega^i < \omega_{max}(i+1)/n$, where $0 \le i < n$ for each band, if no wavevectors at the perimeter of IBZ had corresponding normalized frequency inside the band, and then the value of 1 representing stopband was assigned. Otherwise, the band was represented by the value of 0 and classified as a passband, resulting in a 500-element bandgap vector representing a whole passband–stopband structure. As the second option, we considered a single-valued bandgap ratio ψ as the output. The generated dataset was split into train and test sets in the proportion of 90/10, and we used a relatively simple neural network architecture consisting of 6 hidden layers with 64, 64, 128, 128, 256, and 512 nodes, resulting in approximately 300 000 free parameters to search during training. We have not performed any hyperparameter tuning since here, and the main task was to demonstrate only the feasibility of this approach for considered metamaterials with curvy beams. Figure 5(a) shows the comparison between the real values of ψ obtained by Bloch-Floquet analysis and ψ predicted by the trained model. Note that this model was trained using a bandgap vector as output, however, for the visualization, the bandgap ratio corresponding to the predicted bandgap vector was calculated afterward. In general, one might see the satisfactory quality of the prediction with R^2 score on the test dataset reaching the value of 0.973. In general, predicting the passband–stopband structure is a hard task for neural networks since even for continuous change in the input coordinates, narrow bandgaps can appear and disappear at different frequency ranges. Figure 5(c) shows the comparison between bandgaps found using finite element simulations (red) and predicted by the trained neural network (orange) for the one selected metamaterial with below-average prediction quality. In general, this comparison reveals a good agreement between the bandgap positions and widths. However, it can be observed that the neural network shifts the bandgap to a higher frequency range around $\omega \approx 0.3$ while also merging two separate bandgaps for $0.6 < \omega < 0.7$. The latter is a common mistake, likely associated with the absence of a dispersion branch around $\omega \approx 0.65$ in "neighboring" metamaterials that have values of y_i close to the

considered specimen. Similar to Fig. 5(a), Fig. 5(b) shows the comparison between the true values of ψ obtained by Bloch–Floquet analysis and ψ predicted by the trained model, however, in this case, and the trained model directly takes bandgap ratio ψ as an output. One might see that this model outperforms the previous one reaching $R^2 = 0.991$ on the test dataset, which is expected due to the difference in the learned output. The prediction for a single-valued output model is still non-ideal in part due to opening narrow bandgaps. While we had no goal to achieve the best possible prediction using a neural network, we anticipate that nonstandard loss functions have to be employed for more robust separation between passbands and stopbands during training.

This short letter reveals the benefits of employing curved beams defined by Bezier splines in the design of elastic metamaterials. The switch from classical straight elements to curved ones enables control over bandgap positions and widths while keeping the overall dimensions of the metamaterial constant. The immutability of the dimensions might be very important for applications of elastic metamaterials, enabling very fast replacement of metamaterial-based components in order to fulfill the new requirements. While curved beams offer control over wave propagation, it should be noted that their implementation sacrifices the effective stiffness of the metamaterial. Specifically, lattices assembled from Bezier curves exhibit significantly lower effective Young's modulus when compared to their traditional straight-beam counterparts. Implementation of deep learning to predict passband–stopband structures and, in the future, to generate unit cells with the requested behavior will drastically accelerate the creation process enabling designs of heterogeneous or gradient metamaterials assembled from the unit cells with various shapes. Simultaneously, integrating curved elements into the design of elastic metamaterials might impose constraints on the admissible manufacturing methods. Consequently, it becomes necessary to analyze these limitations and assess the practicality of using Bezier splines in the design of elastic metamaterials for their future development.

AUTHOR DECLARATIONS
Conflict of Interest

The author has no conflicts to disclose.

Author Contributions

Viacheslav Slesarenko: Conceptualization (equal); Data curation (equal); Formal analysis (equal); Funding acquisition (equal); Investigation (equal); Methodology (equal); Project administration (equal); Resources (equal); Software (equal); Supervision (equal); Validation (equal); Visualization (equal); Writing – original draft (equal); Writing – review & editing (equal).

DATA AVAILABILITY

The data that support the findings of this study are available from the corresponding author upon reasonable request.

REFERENCES

[1] M. Kadic, T. Bückmann, R. Schittny, and M. Wegener, Rep. Prog. Phys. **76**, 126501 (2013).

[2] A. O. Krushynska, D. Torrent, A. M. Aragón, R. Ardito, O. R. Bilal, B. Bonello, F. Bosia, Y. Chen, J. Christensen, A. Colombi, S. A. Cummer, B. Djafari-Rouhani, F. Fraternali, P. I. Galich, P. D. Garcia, J.-P. Groby, S. Guenneau, M. R. Haberman, M. I. Hussein, S. Janbaz, N. Jiménez, A. Khelif, V. Laude, M. J. Mirzaali, P. Packo, A. Palermo, Y. Pennec, R. Picó, M. R. López, S. Rudykh, M. Serra-Garcia, C. M. S. Torres, T. A. Starkey, V. Tournat, and O. B. Wright, Nanophotonics **12**, 659 (2023).

[3] D. García-Pablos, M. Sigalas, F. R. Montero de Espinosa, M. Torres, M. Kafesaki, and N. García, Phys. Rev. Lett. **84**, 4349 (2000).

[4] L. D'Alessandro, A. O. Krushynska, R. Ardito, N. M. Pugno, and A. Corigliano, Sci. Rep. **10**, 16403 (2020).

[5] X. Pu, A. Palermo, and A. Marzani, Mech. Syst. Signal Process. **181**, 109478 (2022).

[6] J. U. Surjadi, L. Gao, H. Du, X. Li, X. Xiong, N. X. Fang, and Y. Lu, Adv. Eng. Mater. **21**, 1800864 (2019).

[7] X. Tian, W. Chen, R. Gao, and S. Liu, J. Sound Vib. **500**, 116036 (2021).

[8] Z. Liu, X. Zhang, Y. Mao, Y. Y. Zhu, Z. Yang, C. T. Chan, and P. Sheng, Science **289**, 1734 (2000).

[9] X. Zhou, X. Liu, and G. Hu, Theor. Appl. Mech. Lett. **2**, 041001 (2012).

[10] Y. Chen, T. Li, F. Scarpa, and L. Wang, Phys. Rev. Appl. **7**, 024012 (2017).

[11] V. Slesarenko, P. I. Galich, J. Li, N. X. Fang, and S. Rudykh, Appl. Phys. Lett. **113**, 031901 (2018).

[12] J. Li, V. Slesarenko, and S. Rudykh, Soft Matter **14**, 6171 (2018).

[13] D. Chen, N. Arora, Y. Xiang, J. Li, V. Slesarenko, and S. Rudykh, Mech. Mater. **175**, 104482 (2022).

[14] C. Gao, V. Slesarenko, M. C. Boyce, S. Rudykh, and Y. Li, Sci. Rep. **8**, 11834 (2018).

[15] D. M. Kochmann and K. Bertoldi, Appl. Mech. Rev. **69**, 050801 (2017).

[16] P. I. Galich, A. Sharipova, and S. Slesarenko, Materials **14**, 2038 (2021).

[17] M. Oudich, N. J. Gerard, Y. Deng, and Y. Jing, Adv. Funct. Mater. **33**, 2206309 (2023).

[18] L. Wu, Y. Wang, K. Chuang, F. Wu, Q. Wang, W. Lin, and H. Jiang, Mater. Today **44**, 168 (2021).

[19] D. Wang, H. Xu, J. Wang, C. Jiang, X. Zhu, Q. Ge, and G. Gu, ACS Appl. Mater. Interfaces **12**, 22146 (2020).

[20] W. Wu, W. Hu, G. Qian, H. Liao, X. Xu, and F. Berto, Mater. Des. **180**, 107950 (2019).

[21] S. Mukherjee, M. Cajić, D. Karličić, and S. Adhikari, Compos. Struct. **306**, 116591 (2023).

[22] G. Felsch, N. Ghavidelnia, D. Schwarz, and V. Slesarenko, Comput. Methods Appl. Mech. Eng. **410**, 116032 (2023).

[23] A. Álvarez Trejo, E. Cuan-Urquizo, A. Roman-Flores, L. G. Trapaga-Martinez, and J. M. Alvarado-Orozco, Mater. Des. **199**, 109412 (2021).

[24] T. J. R. Hughes, J. A. Cottrell, and Y. Bazilevs, Comput. Methods Appl. Mech. Eng. **194**, 4135 (2005).

[25] F. Maurin, C. Claeys, E. Deckers, and W. Desmet, Int. J. Solids Struct. **135**, 26 (2018).

[26] Y.-F. Wang, Y.-Z. Wang, B. Wu, W. Chen, and Y.-S. Wang, Appl. Mech. Rev. **72**, 040801 (2020).

[27] Y. Jin, B. Djafari-Rouhani, and D. Torrent, Nanophotonics **8**, 685 (2019).

[28] C.-X. Liu and G.-L. Yu, J. Comput. Des. Eng. **10**, 602 (2023).

[29] Muhammad, J. Kennedy, and C. W. Lim, Mater. Today Commun. **33**, 104606 (2022).